


In Vivo Function of PTEX88 in Malaria Parasite Sequestration and Virulence

Joachim M. Matz,^{a,b,c} Alyssa Ingmundson,^a Jean Costa Nunes,^d Werner Stenzel,^d Kai Matuschewski,^{a,b}  Taco W. A. Kooij^{a,c,e}

Parasitology Unit, Max Planck Institute for Infection Biology, Berlin, Germany^a; Institute of Biology, Humboldt University, Berlin, Germany^b; Department of Medical Microbiology, Radboud Institute for Molecular Life Sciences, Radboud University Medical Centre, Nijmegen, The Netherlands^c; Department of Neuropathology, Charité–Universitätsmedizin, Berlin, Germany^d; Centre for Molecular and Biomolecular Informatics, Radboud Institute for Molecular Life Sciences, Radboud University Medical Centre, Nijmegen, The Netherlands^e

Malaria pathology is linked to remodeling of red blood cells by eukaryotic *Plasmodium* parasites. Central to host cell refurbishment is the trafficking of parasite-encoded virulence factors through the *Plasmodium* translocon of exported proteins (PTEX). Much of our understanding of its function is based on experimental work with cultured *Plasmodium falciparum*, yet direct consequences of PTEX impairment during an infection remain poorly defined. Using the murine malaria model parasite *Plasmodium berghei*, it is shown here that efficient sequestration to the pulmonary, adipose, and brain tissue vasculature is dependent on the PTEX components thioredoxin 2 (TRX2) and PTEX88. While TRX2-deficient parasites remain virulent, PTEX88-deficient parasites no longer sequester in the brain, correlating with abolishment of cerebral complications in infected mice. However, an apparent trade-off for virulence attenuation was spleen enlargement, which correlates with a strongly reduced schizont-to-ring-stage transition. Strikingly, general protein export is unaffected in PTEX88-deficient mutants that mature normally *in vitro*. Thus, PTEX88 is pivotal for tissue sequestration *in vivo*, parasite virulence, and preventing exacerbation of spleen pathology, but these functions do not correlate with general protein export to the host erythrocyte. The presented data suggest that the protein export machinery of *Plasmodium* parasites and their underlying mechanistic features are considerably more complex than previously anticipated and indicate challenges for targeted intervention strategies.

The asexual replication inside the red blood cell is the sole phase of a malaria parasite infection that leads to pathological symptoms (1). Within the host cell, the eukaryotic pathogen hides and replicates in a niche of its own making, termed the parasitophorous vacuole (PV) (2). In order to accommodate the parasite's needs, the erythrocytes are extensively refurbished through the translocation of parasite proteins across the PV membrane into the host cell (3, 4). As a consequence, parasite-derived proteins that are exported to the host cell surface enable the binding to endothelial ligands, thereby preventing free circulation of the infected erythrocytes (1). Through sequestration, the parasite avoids passing the spleen, which otherwise could destroy the infected red blood cell due to the *Plasmodium*-induced changes in rigidity and deformability (5). Sequestration of *Plasmodium falciparum*-infected erythrocytes and the resulting vascular obstruction are responsible for the more severe complications of malaria, including edema, ischemia, and coma (1, 6).

The identification of a protein export element (PEXEL) or vacuolar transport signal (VTS) in *P. falciparum* (7, 8) revealed a large set of exported *Plasmodium* proteins that likely contribute to erythrocyte remodeling and, at least partly, to parasite virulence. The signature PEXEL/VTS motif is strictly conserved among different malaria parasite species. In addition, a growing list of PEXEL/VTS-negative exported proteins (PNEP) is being recognized in *P. falciparum* and other malaria parasite species (9, 10). A corresponding *Plasmodium* translocon of exported proteins (PTEX) (11) is present in all mammalian *Plasmodium* parasites. This specialized multiprotein complex consists of three essential core components (12, 13), two of which have recently been demonstrated to be directly involved in the active export of both PEXEL/VTS-containing proteins and PNEPs (14, 15). In the murine malaria model parasite, *Plasmodium berghei*, two additional

PTEX constituents, thioredoxin 2 (TRX2) and PTEX88, appear to fulfill auxiliary roles (12, 13). While parasites deficient in TRX2 display only minor alterations in growth rate and virulence, PTEX88-deficient parasites could be selected only using advanced experimental genetics approaches (13, 16).

In this study, we systematically investigate the pathology caused by asexual blood-stage *P. berghei* lacking PTEX88 (PBANKA_094130) compared to that caused by TRX2 (PBANKA_135800)-deficient parasites.

MATERIALS AND METHODS

Ethics statement. This study was carried out in strict accordance with the German Tierschutzgesetz in der Fassung vom 22. Juli 2009 and Directive 2010/63/EU of the European Parliament and Council on the Protection of Animals Used for Scientific Purposes. The protocol was approved by the ethics committee of the Berlin state authority (Landesamt für Gesundheit und Soziales Berlin; permit number G0469/09). Female NMRI and C57BL/6 mice were purchased from Charles River Laboratories (Sulzfeld, Germany). NMRI mice were used for blood-stage growth assays and spleen weight measurements. Sporozoite inoculations as well as experi-

Received 11 December 2014 Accepted 25 March 2015

Accepted manuscript posted online 27 March 2015

Citation Matz JM, Ingmundson A, Costa Nunes J, Stenzel W, Matuschewski K, Kooij TWA. 2015. In vivo function of PTEX88 in malaria parasite sequestration and virulence. Eukaryot Cell 14:528–534. doi:10.1128/EC.00276-14.

Address correspondence to Taco W. A. Kooij, Taco.Kooij@radboudumc.nl.

Supplemental material for this article may be found at <http://dx.doi.org/10.1128/EC.00276-14>.

Copyright © 2015, American Society for Microbiology. All Rights Reserved. doi:10.1128/EC.00276-14

mental cerebral malaria (ECM) and sequestration experiments were performed using C57BL/6 mice.

***Plasmodium berghei* in vivo and ex vivo blood-stage development.**

For *ex vivo* cultivation of *P. berghei*, blood from highly infected mice (2 to 5%) was collected and incubated in *P. berghei* culture medium (RPMI 1640 complemented with 20% heat-inactivated fetal calf serum [FCS]). The cultures were incubated in a low-oxygen atmosphere (5%) at 37°C under constant shaking (77 rpm). In order to obtain a synchronized *P. berghei* infection, schizont purification was performed 18 h after inoculation by one-step Nycodenz density gradient centrifugation (17). The obtained schizont pellets were resuspended in medium and intravenously injected into recipient mice for highly synchronized *in vivo* infections. To obtain tightly synchronized *ex vivo* cultures, blood from these mice was collected 1 h after schizont injection and incubated once more in *P. berghei* culture medium. Stage determination of synchronized *ex vivo* cultures and *in vivo* infections of wild-type (WT) (Bergreen) (13), *trx2*⁻, and *ptex88*⁻ parasites was performed by microscopic examination of Giemsa-stained thin films.

In order to measure the stage conversion efficiency of tightly synchronized, *ex vivo*-cultured schizonts, NMRI donor mice were infected with both *ptex88*⁻ parasites and yellow fluorescent protein (YFP)-expressing WT (Beryellow) parasites (13). The parasitemias of the two parasite populations were measured by flow cytometry prior to inoculation of an *ex vivo* blood culture for schizont or merozoite purification. Two hours following the injection of the mixed purified schizonts or released merozoites into recipient mice, the parasitemias were measured again to compare stage conversion of the two parasite lines.

Mouse pathogenesis and histology. In order to determine the outcome of a blood-stage infection, 1,000 WT (Bergreen), 1,000 *trx2*⁻, 5,000 *trx2*⁻, 1,000 *ptex88*⁻, or 100,000 *ptex88*⁻ parasites were injected intravenously into naive C57BL/6 mice. Development of cerebral complications was monitored daily by assessing behavioral and functional abnormalities (18). Upon the diagnosis of a minimum of three neurological symptoms, usually between 7 and 9 days after injection, mice were classified as suffering from ECM and sacrificed. For quantification of the parasite burden by real-time PCR and histology, highly infected C57BL/6 mice were sacrificed 7 days after injection. The animals were perfused intracardially with isotonic NaCl solution. Brains, lungs, and adipose tissue were harvested and either fixed for 48 h in 4% buffered formaldehyde or homogenized in TRIzol for RNA isolation and subsequent cDNA synthesis and real-time PCR. After paraffin embedding, 4- μ m tissue sections were stained with Giemsa (adipose tissue), an anti-green fluorescent protein (GFP) antibody (lungs and brains; Abcam, United Kingdom), or hematoxylin and eosin (H&E; brain). Microglial cells were visualized by using an anti-ionized calcium-binding adapter molecule 1 (IBA1) antibody (WAKO, Japan). Astrocytes were stained with an anti-gial fibrillary acidic protein (GFAP) antibody (Dako, Germany). The immunohistochemical staining procedures were performed by using the iView-Ventana diaminobenzidine (DAB) detection kit (Ventana, Tucson, AZ, USA) with appropriate biotinylated secondary antibodies and DAB visualization of the peroxidase reaction product with a Benchmark XT immunostainer (Ventana). The omission of primary antibodies resulted in the absence of any cellular labeling. Photomicrographs were taken with a Leica DMR microscope equipped with a Jenoptik ProgRes SpeedXT Core 3 charge-coupled device (CCD) camera. For spleen weight measurements, NMRI mice were sacrificed 1 week after the injection of 1,000 parasites. Splenectomies for the *in vivo* growth assay were performed in NMRI mice several weeks before parasite injection.

Assessment of protein export. The surface antigen labeling of infected erythrocytes was performed using serum from a naive mouse or from a mouse immunized with blood-stage parasites (15, 19). A single drop of tail blood was taken from a WT (Bergreen)- or *ptex88*⁻-infected mouse. Erythrocytes were washed briefly in RPMI 1640 (Gibco) and blocked in *P. berghei* culture medium for 45 min before 3 h of incubation with 20% semi- or nonimmune serum in RPMI. After repeated washing with *P.*

berghei culture medium, the cells were incubated for 2 h with secondary antibody (Alexa Fluor 546 goat anti-mouse; 1:250; Life Technologies). After thorough washing, fluorescence was detected with a Zeiss AxioObserver Z1 epifluorescence microscope. A similar protocol was used for flow-cytometric analysis, using blood from a double-infected mouse (WT [Beryellow] and *ptex88*⁻ parasites) and a different secondary antibody (Alexa Fluor 633 goat anti-mouse; 1:250; Life Technologies). Fluorescence of infected cells was measured by flow cytometry using a BD Biosciences LSR Fortessa analyzer. All incubations were carried out at room temperature.

For live localization of cargo proteins, transgenic parasite lines were generated by single-crossover homologous recombination (see Fig. S1A and Table S1 in the supplemental material). Transfection constructs were made by introducing the PCR-amplified carboxy-terminal sequences (in some cases, including the adjacent 5' flanking sequence) into the b3D+mCherry vector (20) using the SacII and SpeI/NheI recognition sites (see Table S1). Vectors were linearized in the coding sequence, using BstBI (PBANKA_144540), BsmI (PBANKA_083680), PmlI (PBANKA_021540), PacI (PBANKA_010060), XbaI (PBANKA_132730), or SpeI (PBANKA_140030), and transfected into *P. berghei* strain ANKA parasites using the standard procedure (17). After successful transfection, the parasites harbored a carboxy-terminal mCherry tag in the respective endogenous locus. Successful integration was confirmed by fluorescence and diagnostic PCR (see Fig. S1B and Table S1). For live localization studies of PBANKA_136550, the *IBIS1-mCherry* parasite line was used (21). All seven parasite lines expressing mCherry-tagged cargo proteins were crossed *in vivo* with the *ptex88*⁻ parasites. Single and double mutants were imaged live following bite-back feeding to C57BL/6 mice.

Statistical analysis. All data were obtained from at least 3 independent experiments (shown are mean values \pm standard deviations [SD]). The statistical analyses were performed using GraphPad Prism 5.0 software. All parasite blood-stage development experiments were analyzed using two-way analysis of variance (ANOVA). Data from the exponential growth phase, i.e., with parasitemia of <1%, fitted a linear regression well ($r^2 \geq 0.99$) and allowed the calculation and comparison of the parasite multiplication rates. Differences in time to development of ECM symptoms were analyzed using the Mantel-Cox test. Schizont nuclei were compared using an unpaired two-tailed Student's *t* test of the cohorts of schizonts harboring >8 nuclei. All other data sets were analyzed with a one-way ANOVA followed by Tukey's multiple-comparison test. *P* values of <0.05 were considered statistically significant.

RESULTS

Absence of PTEX88 and thioredoxin 2 impairs tissue sequestration of *Plasmodium berghei*-infected erythrocytes. Upon inspection of the parasitemias of infected mice, we observed that *ptex88*⁻ parasites displayed elevated numbers of schizonts in the peripheral blood (Fig. 1A). This prompted us to carefully monitor the course of synchronized *in vivo* blood infections (Fig. 1B). We detected a remarkably high (30%) percentage of schizonts in the peripheral blood of *ptex88*⁻-infected animals compared to that in WT infections (3%). This phenomenon was most pronounced 22 h after infection and coincided with a reduced sequestration-dependent drop in parasitemia during parasite maturation (Fig. 1C). In comparison, *trx2*⁻ parasites displayed an intermediate phenotype.

Previous work established that *P. berghei* schizonts typically sequester to adipose and lung tissue (22, 23), which also was recently documented in *P. falciparum*-infected patients (24). To test whether the large proportion of circulating *ptex88*⁻ schizonts correlates with a defect in sequestration, we analyzed histological organ sections of infected mice adjusted to similar parasitemia levels (Fig. 2A). The number of sequestered parasites in the pulmonary vessels was an order of magnitude lower during an infection with

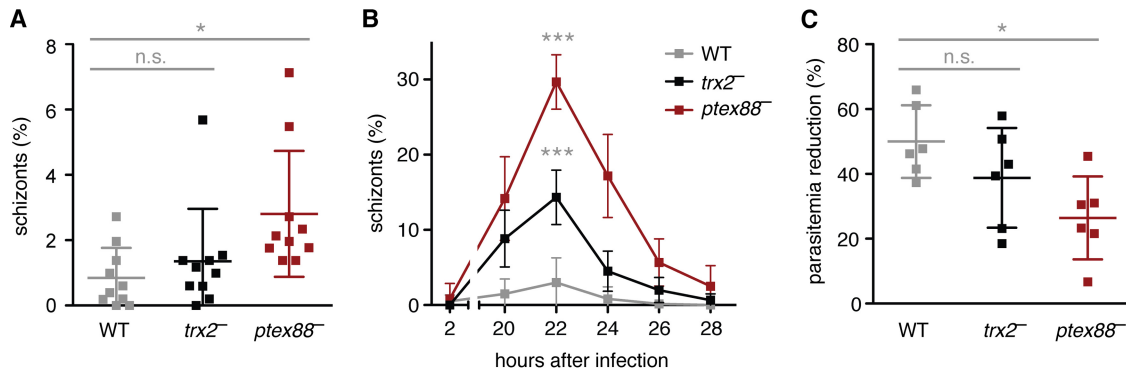


FIG 1 Ablations of *PTEX88* and *TRX2* lead to enhanced schizont circulation *in vivo*. (A) Proportion of schizont-infected erythrocytes in peripheral blood during asynchronous infections with WT (gray), *trx2*⁻ (black), and *ptex88*⁻ (red) parasites (n.s., nonsignificant; *, $P < 0.05$; one-way ANOVA and Tukey's multiple-comparison test; $n = 10$). (B) Proportion of schizont-infected erythrocytes in peripheral blood during tightly synchronized infections with WT (gray), *trx2*⁻ (black), and *ptex88*⁻ (red) parasites (***, $P < 0.001$; two-way ANOVA; $n = 6$). (C) Parasitemias of tightly synchronized infections were measured 2 h (all rings) and 20 h (all mature stages) after injection of WT (gray), *trx2*⁻ (black), and *ptex88*⁻ (red) schizonts. The reduction of parasitemia coincides with the dominance of mature stages and the absence of ring-stage parasites (n.s., nonsignificant; *, $P < 0.05$; one-way ANOVA and Tukey's multiple-comparison test; $n = 6$).

ptex88⁻ parasites than in WT infections (Fig. 2B). This defect is even more pronounced in adipose tissue, where only very few *ptex88*⁻ schizonts were detected (Fig. 2C). As expected, ablation of *TRX2* resulted in a more moderate reduction of the parasite burden in vessels of lung and adipose tissue (Fig. 2B and C). Molecular analysis of parasite rRNA by quantitative PCR (qPCR) reflects the results of the histological quantification (see Fig. S2A and B in the supplemental material), although incomplete perfusion, for instance, of fat tissue, renders the differences less prominent than in histology, which permits cell type-specific quantifications.

***ptex88*⁻ parasites do not cause experimental cerebral malaria.** A lethal outcome of infections with virulent *P. berghei* (strain ANKA) is ECM (25). Although a link between sequestration of infected erythrocytes in the brain and ECM is plausible, experimental evidence for such a correlation remains controversial (22, 26). Histological sections of infected C57BL/6 mice 7 days after infection revealed a 6-fold reduction in sequestration of *ptex88*⁻-infected erythrocytes in the brain capillaries (Fig. 3A and B). In contrast, *trx2*⁻ parasites displayed a less striking deficit, resulting in a substantial, albeit nonsignificant, reduction in parasite burden in the cerebral vessels (Fig. 3A and B). Differences in cerebral parasite burden could not be confirmed using real-time PCR, probably due to remaining blood in hemorrhages and larger vessels (see Fig. S2C in the supplemental material).

To establish a potential link between the striking sequestration deficit of the *ptex88*⁻ mutant and parasite virulence, we investigated the infection outcome by monitoring the development of ECM in C57BL/6 mice following the intravenous injection of 1,000 parasites. We compared the development of cerebral complications during infections with WT, *ptex88*⁻, and *trx2*⁻ parasites (Fig. 3C). Strikingly, all *ptex88*⁻-infected mice remained ECM free and continued to develop hyperparasitemia and anemia during the later phase of infection. Even when a 100-fold excess of *ptex88*⁻ parasites was injected, no signature ECM symptoms were observed. In contrast, 80% of *trx2*⁻-infected animals displayed symptoms of cerebral complications.

We next performed a histological analysis of cerebral bleeding and activation of microglia and astrocytes (see Fig. S3 in the supplemental material). We note that histological samples from

ptex88⁻, *trx2*⁻, and WT-infected mice were indistinguishable 7 days after infection. Apparently, continuous parasite replication in the peripheral blood elicits damage to the host, including tissue injury. This finding is reminiscent of asymptomatic infections of A/J mice with either virulent (ANKA) or avirulent (NK65) *P. berghei*, which in both cases leads to cerebral hemorrhages but not ECM (26).

General export of parasite proteins is unaffected in *ptex88*⁻ parasites. Sequestration and virulence might be dependent on a functioning protein export machinery. Therefore, we tested whether *ptex88*⁻ parasites displayed defects in the export of virulence factors to the red blood cell surface by staining with serum from an immunized mouse. Surprisingly, we did not detect any significant differences in antigen exposure between WT- and *ptex88*⁻-infected erythrocytes (Fig. 4A and B). To obtain independent support for our finding, we also analyzed the localization of seven exported proteins representing four known classes, i.e., proteins with a PEXEL/VTS motif, PNEPs, with and without transmembrane domains (Fig. 4C; also see Fig. S1 in the supplemental material). In agreement with the results from the surface labeling, no deficits in export were observed. All cargo proteins were targeted to the cytoplasm or to the periphery of the erythrocyte, including the schizont membrane-associated cytoadherence protein (SMAC), which is required for efficient tissue sequestration (27).

It has been demonstrated previously that inhibition of protein export by conditional knockdown of PTEX core components resulted in a growth arrest during asexual blood-stage propagation (14, 15). Therefore, we tested whether the overall slower blood-stage development of the *ptex88*⁻ mutant can be attributed to delayed parasite maturation. We inoculated synchronized *ex vivo* blood cultures and assessed the parasite stages by microscopic analysis of Giemsa-stained culture smears (Fig. 5A; also see Fig. S4 in the supplemental material). There were no detectable differences in the stage distribution of WT and *ptex88*⁻ parasites, further strengthening the notion of general protein export competence in the *PTEX88*-deficient mutant. In contrast, *trx2*⁻ parasites developed significantly slower and displayed prolonged persistence of trophozoites and fewer nuclei per schizont, which is in

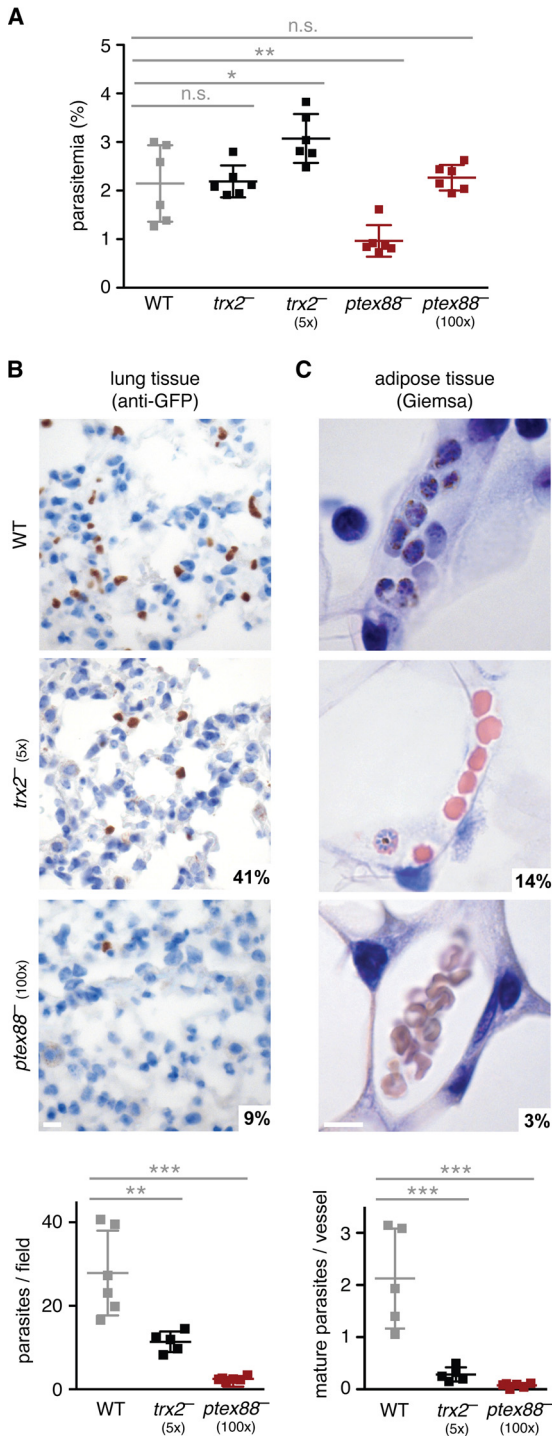


FIG 2 *PTEX88* and *TRX2* are important for efficient sequestration to lung and adipose tissue. (A) Parasitemias on day 7 after intravenous injection of 1,000, 5,000 (5×), or 100,000 (100×) parasites (n.s., nonsignificant; *, $P < 0.05$; **, $P < 0.01$; one-way ANOVA and Tukey's multiple-comparison test; $n = 6$). Representative micrographs of lung (B) and adipose (C) tissue infected with WT (top), *trx2*⁻ (center), and *ptex88*⁻ (bottom) parasites are shown. Parasites were visualized by immunohistochemistry using an anti-GFP antibody (lung tissue) or stained with Giemsa (adipose tissue) and quantified microscopically (graphs; **, $P < 0.01$; ***, $P < 0.001$; one-way ANOVA and Tukey's multiple-comparison test; $n \geq 5$). Bar, 10 μ m.

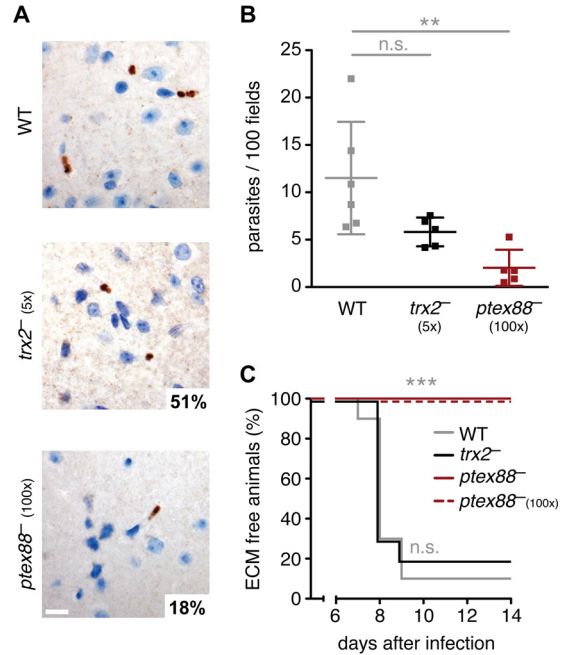


FIG 3 Reduced cerebral sequestration of *ptex88*⁻ parasites correlates with absence of experimental cerebral malaria. (A) Representative micrographs of brain tissue infected with WT (top), *trx2*⁻ (center), and *ptex88*⁻ (bottom) parasites. Parasites were visualized by immunohistochemistry using an anti-GFP antibody. Bar, 10 μ m. (B) Microscopic quantification of sequestered parasites in cerebral vessels (n.s., nonsignificant; **, $P < 0.01$; one-way ANOVA and Tukey's multiple-comparison test; $n \geq 5$). (C) Kaplan-Meier analysis of time to development of signature experimental cerebral malaria (ECM) symptoms. C57BL/6 mice were infected by intravenous injection of 1,000 WT (gray), *trx2*⁻ (black), or *ptex88*⁻ blood-stage parasites (red solid line) or by injection of 100,000 *ptex88*⁻ (100×, red dashed line) parasites (***, $P < 0.001$; Mantel-Cox test; $n = 10$).

good agreement with its slightly reduced blood-stage propagation rate (12, 13) and protein export deficiency (15).

Splenomegaly in *ptex88*⁻-infected mice. During organ extractions, we observed a remarkable swelling of the spleen in *ptex88*⁻-infected mice. We quantified this by measuring the splenic mass of NMRI mice 7 days after intravenous injection of 1,000 infected erythrocytes (Fig. 5B). *ptex88*⁻-infected mice displayed clear signs of exacerbated splenomegaly. Notably, this pathology coincides with the 2-fold lower parasitemias of *ptex88*⁻-infected mice compared to that of WT-infected animals at this time point (Fig. 2A).

Splenic clearance is considered the principal mechanism to remove infected erythrocytes and nonviable parasites from the circulation and frequently results in splenomegaly (5). To investigate the possibility that the growth deficit observed in *ptex88*⁻ parasites is due directly to enhanced splenic clearance of circulating mature parasite stages, we infected splenectomized animals (Fig. 5C). Blood-stage development of both *ptex88*⁻ and WT parasites was not significantly affected by splenectomy, corroborating earlier findings with *P. berghei* parasites lacking the exported protein SMAC (27).

Spleen swelling could be due to recognition of nonviable *ptex88*⁻ parasites. Since we did not observe enhanced mortality during parasite maturation (Fig. 5A), we looked for deficiencies during the schizont-to-ring-stage transition by injection of puri-

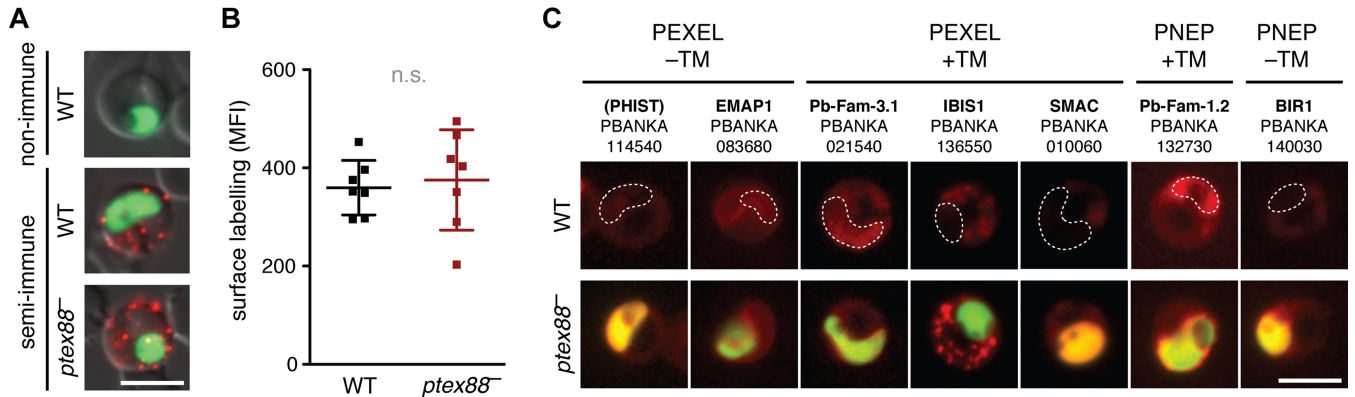


FIG 4 General export of parasite proteins is unaffected in *ptex88*⁻ parasites. (A) Surface labeling of parasite-derived antigens on WT (top)- and *ptex88*⁻ (bottom)-infected erythrocytes by live immunofluorescence using sera of nonimmune and semi-immune mice. Depicted is a merge of the stained antigens (red), the parasite cytoplasm (green), and a differential interference contrast image. Bar, 5 μ m. (B) Quantification of parasite-derived antigens on the surface of WT- and *ptex88*⁻ infected erythrocytes. Shown is the mean fluorescence intensity (MFI) as determined by flow-cytometric analysis after staining with semi-immune serum (n.s., nonsignificant; paired Student's *t* test; *n* = 7). (C) Live imaging of representative mCherry-tagged cargo proteins (red signal) in WT (top)- and *ptex88*⁻ (bottom)-infected erythrocytes. The white outline marks the position of the nonfluorescent WT parasites. *ptex88*⁻ parasites can be recognized by their cytoplasmic GFP fluorescence. Note that *ptex88*⁻ parasites display a certain degree of cytoplasmic mCherry fluorescence due to promoter tagging in the original loss-of-function mutant (13). Names and locus tag numbers of the exported proteins are shown. PEXEL, *Plasmodium* export element; PNEP, PEXEL-negative exported protein; TM, transmembrane domain. Bar, 5 μ m.

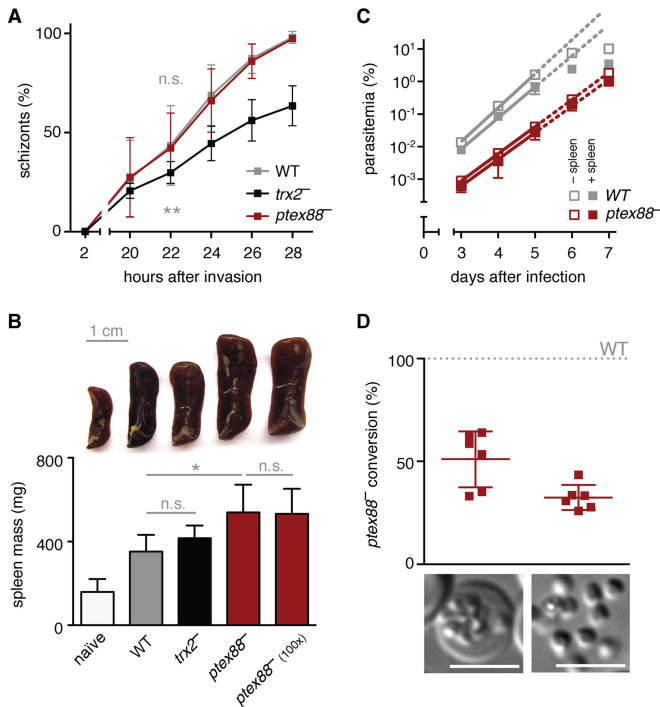


FIG 5 Impaired schizont-to-ring-stage transition of *ptex88*⁻ parasites correlates with exacerbated splenomegaly in infected mice. (A) *ptex88*⁻ parasites develop normally *ex vivo*, while *trx2*⁻ parasites display a continuous growth delay (n.s., nonsignificant; **, *P* < 0.01; two-way ANOVA; *n* = 6). (B) Representative photographs of spleens (top, from left to right) from a naive mouse, a WT-infected mouse, a *trx2*⁻ infected mouse, and two *ptex88*⁻ infected mice (1 \times and 100 \times inoculum). Shown below is spleen weight (milligrams) according to infection. Spleens were removed 7 days after intravenous injection of 1,000 or 100,000 (100 \times) parasites (n.s., nonsignificant; *, *P* < 0.05; one-way ANOVA and Tukey's multiple-comparison test; *n* = 5). (C) *In vivo* parasite growth of WT (gray) and *ptex88*⁻ (red) parasites in normal (filled squares) or splenectomized (open squares) mice (nonsignificant; two-way ANOVA; *n* = 3). Parasite multiplication rates were the following: WT, normal mice, 9.1; WT, splenectomized mice, 11.0; *ptex88*⁻, normal mice, 6.6; *ptex88*⁻, splenectomized mice, 6.8. (D) *In vivo* schizont-to-ring-stage conversion of *ex vivo*-cultured *ptex88*⁻ parasites relative to an internal WT control after mixed inoculations of schizonts (left) or free merozoites (right). Bars, 5 μ m.

infected schizonts (Fig. 5D). We observed a 2-fold drop in relative *ptex88*⁻ parasitemia, suggesting that reduced parasite multiplication can be attributed largely to this step of the asexual replication cycle. Since a similar drop in stage conversion efficiency was observed when purified merozoites were injected, a potential defect in parasite egress is unlikely.

DISCUSSION

In this study, we provide the first *in vivo* evidence for functions of PTEX components in the sequestration of infected erythrocytes to multiple organs. The reduced presence of *ptex88*⁻ parasites in cerebral vessels correlates with the complete loss of ECM symptoms and lends additional support to the critical interrelation of tissue sequestration and parasite virulence. In contrast, *trx2*⁻ infected mice were prone to a lethal disease outcome, underlining an earlier study, which reported incomplete levels of protection from ECM in *trx2*⁻ infected animals (12).

These differences in clinical outcome match our data on tissue sequestration, which is only moderately reduced for *trx2*⁻ parasites and much more pronounced in *ptex88*⁻ mutants. However, whereas *trx2*⁻ parasites were shown to exhibit suboptimal protein export (15), we were not able to detect such a defect in parasites lacking PTEX88. Our finding that protein export remains unaffected in *ptex88*⁻ parasites casts considerable doubt that this protein is involved in the actual translocation process. To date, the only supporting evidence for this has been biochemical data from coimmunoprecipitation experiments (11). Still, the defects in parasite sequestration and virulence upon PTEX88 deletion are striking, suggesting important, albeit undisclosed, roles in erythrocyte remodeling. We note that we cannot formally exclude that translocation of a few selected cargo proteins strictly depends on PTEX88. We consider this scenario rather unlikely, since exported proteins share common features, regardless of their targeting motives (9, 28). An alternative, but highly speculative, explanation is that PTEX88 acts primarily in modifying, and thereby functionalizing, proteins prior to export without affecting translocation itself.

We also show that PTEX88-deficient parasites mature nor-

mally and display a defect in schizont-to-ring-stage conversion. One explanation is that the merozoites suffer from a specific invasion defect. This would be difficult to reconcile with the original identification as part of the PTEX translocon. A second explanation could be that the microenvironment created during sequestration is directly beneficial for parasite replication (29) or reinvasion by bringing mature merozoites in close proximity to new host erythrocytes in a more static setting. Based on our observations, we favor the hypothesis that PTEX88 performs more specialized functions, particularly around the time of sequestration, that in turn affect the mature parasite stages and, as a result, merozoite viability. Circulating nonviable merozoites may well be the cause for the shift in pathology to splenomegaly. Indeed, our inability to recover WT-like multiplication rates in splenectomized mice suggests that spleen swelling in *ptex88*⁻-infected mice is not associated with clearance of viable nonsequestering *ptex88*⁻ parasites.

Splenomegaly is a hallmark of malaria in human and murine infections that remains understudied (1, 5). Therefore, our *in vivo* model also might offer research opportunities toward a better understanding of the pathophysiology of splenomegaly observed in persisting human malaria.

Our findings in the murine malaria model show that complete virulence attenuation and a clinical benefit against severe disease progression can be achieved by ablating PTEX88 function. The associated increase in spleen pathology, however, warrants a cautionary note; tailored intervention strategies that target the malaria parasite's PTEX components might be more difficult to develop than previously anticipated, since partial parasite survival might give rise to unforeseen complications.

ACKNOWLEDGMENTS

We thank Carolin Rauch, Manuel Rauch, Petra Matylewski, and Silke Bandermann for technical assistance. We also acknowledge the assistance of the Flow Cytometry Core Facility at the Deutsches Rheuma-Forschungszentrum (Berlin), particularly Toralf Kaiser and Jenny Kirsch, for expert advice.

This work was supported by the Max Planck Society and partly by the European Commission through the EVIMalaR network (partner 34).

REFERENCES

- Haldar K, Murphy SC, Milner DA, Taylor TE. 2007. Malaria: mechanisms of erythrocytic infection and pathological correlates of severe disease. *Annu Rev Pathol* 2:217–249. <http://dx.doi.org/10.1146/annurev.pathol.2.010506.091913>.
- Spielmann T, Montagna GN, Hecht L, Matuschewski K. 2012. Molecular make-up of the *Plasmodium* parasitophorous vacuolar membrane. *Int J Med Microbiol* 302:179–186. <http://dx.doi.org/10.1016/j.ijmm.2012.07.011>.
- Boddey JA, Cowman AF. 2013. *Plasmodium* nesting: remaking the erythrocyte from the inside out. *Annu Rev Microbiol* 67:243–269. <http://dx.doi.org/10.1146/annurev-micro-092412-155730>.
- Maier AG, Rug M, O'Neill MT, Brown M, Chakravorty S, Szestak T, Chesson J, Wu Y, Hughes K, Coppel RL, Newbold C, Beeson JG, Craig A, Crabb BS, Cowman AF. 2008. Exported proteins required for virulence and rigidity of *Plasmodium falciparum*-infected human erythrocytes. *Cell* 134:48–61. <http://dx.doi.org/10.1016/j.cell.2008.04.051>.
- del Portillo HA, Ferrer M, Brugat T, Martin-Jaular L, Langhorne J, Lacerda MVG. 2012. The role of the spleen in malaria. *Cell Microbiol* 14:343–355. <http://dx.doi.org/10.1111/j.1462-5822.2011.01741.x>.
- Ponsford MJ, Medana IM, Prapansilp P, Hien TT, Lee SJ, Dondorp AM, Esiri MM, Day NPJ, White NJ, Turner GDH. 2012. Sequestration and microvascular congestion are associated with coma in human cerebral malaria. *J Infect Dis* 205:663–671. <http://dx.doi.org/10.1093/infdis/jir812>.
- Hillier NL, Bhattacharjee S, van Ooij C, Liolios K, Harrison T, Lopez-Estraño C, Haldar K. 2004. A host-targeting signal in virulence proteins reveals a secretome in malarial infection. *Science* 306:1934–1937. <http://dx.doi.org/10.1126/science.1102737>.
- Marti M, Good RT, Rug M, Knuepfer E, Cowman AF. 2004. Targeting malaria virulence and remodeling proteins to the host erythrocyte. *Science* 306:1930–1933. <http://dx.doi.org/10.1126/science.1102452>.
- Grüiring C, Heiber A, Kruse F, Flemming S, Franci G, Colombo SF, Fasana E, Schoeler H, Borgese N, Stunnenberg HG, Przyborski JM, Gilberger T-W, Spielmann T. 2012. Uncovering common principles in protein export of malaria parasites. *Cell Host Microbe* 12:717–729. <http://dx.doi.org/10.1016/j.chom.2012.09.010>.
- Pasini EM, Braks JA, Fonager J, Klop O, Aime E, Spaccapelo R, Otto TD, Berriman M, Hiss JA, Thomas AW, Mann M, Janse C, Kocken CHM, Franke-Fayard B. 2013. Proteomic and genetic analyses demonstrate that *Plasmodium berghei* blood stages export a large and diverse repertoire of proteins. *Mol Cell Proteomics* 12:426–448. <http://dx.doi.org/10.1074/mcp.M112.021238>.
- de Koning-Ward TF, Gilson PR, Boddey JA, Rug M, Smith BJ, Papenfuss AT, Sanders PR, Lundie RJ, Maier AG, Cowman AF, Crabb BS. 2009. A newly discovered protein export machine in malaria parasites. *Nature* 459:945–949. <http://dx.doi.org/10.1038/nature08104>.
- Matthews K, Kalanon M, Chisholm SA, Sturm A, Goodman CD, Dixon MWA, Sanders PR, Nebl T, Fraser F, Haase S, McFadden GI, Gilson PR, Crabb BS, de Koning-Ward TF. 2013. The *Plasmodium* translocon of exported proteins (PTEX) component thioredoxin-2 is important for maintaining normal blood-stage growth. *Mol Microbiol* 89:1167–1186. <http://dx.doi.org/10.1111/mmi.12334>.
- Matz JM, Matuschewski K, Kooij TWA. 2013. Two putative protein export regulators promote *Plasmodium* blood stage development *in vivo*. *Mol Biochem Parasitol* 191:44–52. <http://dx.doi.org/10.1016/j.molbiopara.2013.09.003>.
- Beck JR, Muralidharan V, Oksman A, Goldberg DE. 2014. PTEX component HSP101 mediates export of diverse malaria effectors into host erythrocytes. *Nature* 511:592–595. <http://dx.doi.org/10.1038/nature13574>.
- Elsworth B, Matthews K, Nie CQ, Kalanon M, Charnaud SC, Sanders PR, Chisholm SA, Counihan NA, Shaw PJ, Pino P, Chan J-A, Azevedo MF, Rogerson SJ, Beeson JG, Crabb BS, Gilson PR, de Koning-Ward TF. 2014. PTEX is an essential nexus for protein export in malaria parasites. *Nature* 511:587–591. <http://dx.doi.org/10.1038/nature13555>.
- Matz JM, Kooij TWA. 2015. Towards genome-wide experimental genetics in the *in vivo* malaria model parasite *Plasmodium berghei*. *Pathog Glob Health* 109:46–60. <http://dx.doi.org/10.1179/204773215Y.0000000006>.
- Janse C, Franke-Fayard B, Mair GR, Ramesar J, Thiel C, Engelmann S, Matuschewski K, van Gemert G-J, Sauerwein RW, Waters AP. 2006. High efficiency transfection of *Plasmodium berghei* facilitates novel selection procedures. *Mol Biochem Parasitol* 145:60–70. <http://dx.doi.org/10.1016/j.molbiopara.2005.09.007>.
- Lackner P, Beer R, Heussler V, Goebel G, Rudzki D, Helbok R, Tannich E, Schmutzhard E. 2006. Behavioural and histopathological alterations in mice with cerebral malaria. *Neuropathol Appl Neurobiol* 32:177–188. <http://dx.doi.org/10.1111/j.1365-2990.2006.00706.x>.
- de Koning-Ward TF, O'Donnell RA, Drew DR, Thomson R, Speed TP, Crabb BS. 2003. A new rodent model to assess blood stage immunity to the *Plasmodium falciparum* antigen merozoite surface protein 1₉ reveals a protective role for invasion inhibitory antibodies. *J Exp Med* 198:869–875. <http://dx.doi.org/10.1084/jem.20030085>.
- Silvie O, Goetz K, Matuschewski K. 2008. A sporozoite asparagine-rich protein controls initiation of *Plasmodium* liver stage development. *PLoS Pathog* 4:e1000086. <http://dx.doi.org/10.1371/journal.ppat.1000086>.
- Ingmundson A, Nahar C, Brinkmann V, Lehmann MJ, Matuschewski K. 2012. The exported protein *Plasmodium berghei* protein IBIS1 delineates membranous structures in infected red blood cells. *Mol Microbiol* 83:1229–1243. <http://dx.doi.org/10.1111/j.1365-2958.2012.08004.x>.
- Franke-Fayard BMD, Janse C, Cunha-Rodrigues M, Ramesar J, Büscher P, Que I, Löwik C, Voshol PJ, Boer den MAM, van Duinen SG, Febbraio M, Mota MM, Waters AP. 2005. Murine malaria parasite sequestration: CD36 is the major receptor, but cerebral pathology is unlinked to sequestration. *Proc Natl Acad Sci U S A* 102:11468–11473. <http://dx.doi.org/10.1073/pnas.0503386102>.
- Franke-Fayard B, Fonager J, Braks A, Khan SM, Janse C. 2010. Sequestration and tissue accumulation of human malaria parasites: can we learn anything from rodent models of malaria? *PLoS Pathog* 6:e1001032. <http://dx.doi.org/10.1371/journal.ppat.1001032>.
- Milner DA, Whitten RO, Kamiza S, Carr R, Liomba G, Dzamalala C,

- Seydel KB, Molyneux ME, Taylor TE. 2014. The systemic pathology of cerebral malaria in African children. *Front Cell Infect Microbiol* 4:104. <http://dx.doi.org/10.3389/fcimb.2014.00104>.
25. Engwerda C, Belnoue E, Grüner AC, Rénia L. 2005. Experimental models of cerebral malaria. *Curr Top Microbiol Immunol* 297:103–143.
26. Nacer A, Movila A, Baer K, Mikolajczak SA, Kappe SHI, Frevert U. 2012. Neuroimmunological blood brain barrier opening in experimental cerebral malaria. *PLoS Pathog* 8:e1002982. <http://dx.doi.org/10.1371/journal.ppat.1002982>.
27. Fonager J, Pasini EM, Braks JAM, Klop O, Ramesar J, Remarque EJ, Vroegrijk IOCM, van Duinen SG, Thomas AW, Khan SM, Mann M, Kocken CHM, Janse C, Franke-Fayard BMD. 2012. Reduced CD36-dependent tissue sequestration of *Plasmodium*-infected erythrocytes is detrimental to malaria parasite growth *in vivo*. *J Exp Med* 209:93–107. <http://dx.doi.org/10.1084/jem.20110762>.
28. Heiber A, Kruse F, Pick C, Grüring C, Flemming S, Oberli A, Schoeler H, Retzlaff S, Mesén-Ramírez P, Hiss JA, Kadekoppala M, Hecht L, Holder AA, Gilberger T-W, Spielmann T. 2013. Identification of new PNEPs indicates a substantial non-PEXEL exportome and underpins common features in *Plasmodium falciparum* protein export. *PLoS Pathog* 9:e1003546. <http://dx.doi.org/10.1371/journal.ppat.1003546>.
29. Sherman IW, Eda S, Winograd E. 2003. Cytoadherence and sequestration in *Plasmodium falciparum*: defining the ties that bind. *Microbes Infect* 5:897–909. [http://dx.doi.org/10.1016/S1286-4579\(03\)00162-X](http://dx.doi.org/10.1016/S1286-4579(03)00162-X).